

Computations of primordial black hole formation

Ilia Musco¹, John C. Miller^{1,2} and Luciano Rezzolla^{1,3}

¹ SISSA, International School for Advanced Studies and INFN, Via Beirut 2-4, 34014 Trieste, Italy;

² Department of Physics (Astrophysics), University of Oxford, Keble Road, Oxford OX1 3RH, England;

³ Department of Physics, Louisiana State University, Baton Rouge, LA 70803, USA.

Abstract. Results are presented from general relativistic numerical computations of primordial black-hole formation during the radiation-dominated era of the universe. Growing-mode perturbations are specified within the linear regime and their subsequent evolution is followed as they become nonlinear. We use a spherically symmetric Lagrangian code and study both super-critical perturbations, which go on to produce black holes, and sub-critical perturbations, for which the overdensity eventually disperses into the background medium. For super-critical perturbations, we confirm the results of previous work concerning scaling-laws but note that the threshold amplitude for a perturbation to lead to black-hole formation is substantially reduced when the initial conditions are taken to represent purely growing modes. For sub-critical cases, where an initial collapse is followed by a subsequent re-expansion, strong compressions and rarefactions are seen for perturbation amplitudes near to the threshold. We have also investigated the effect of including a significant component of vacuum energy and have calculated the resulting changes in the threshold and in the slope of the scaling law.

22 October 2018

1. Introduction

Cosmological structure formation is thought to have resulted from the growth and evolution of small perturbations initiated at the time of inflation (see [1] and references therein). Inflationary models give rise to a spectrum of fluctuations on scales larger

than the cosmological horizon which then start to re-enter the horizon in the radiation-dominated era. Primordial black holes (PBHs) could be formed at this stage in extreme cases where the fluctuation amplitude exceeds a critical threshold value [2, 3, 4]. The masses of these PBHs could, in principle, span many orders of magnitude, from the Planck mass up to the horizon mass at the time of equivalence between radiation and matter ($\sim 10^4$ years after the Big Bang).

Sufficiently small PBHs would have emitted a significant amount of Hawking radiation and, according to the standard picture, would have evaporated completely away before now if their mass was less than $\sim 10^{15}$ g. It has been suggested that extremely small PBHs of $\sim 10^5 - 10^6$ g, formed in the very early Universe, might have been the cause of baryogenesis [5], while PBHs of $\sim 10^{15}$ g evaporating now might explain a class of observed very short-duration gamma ray bursts [6, 7, 8] and some cosmic rays [9, 10]. It has also been suggested that the evaporation of small black holes might not continue all the way to zero mass but might stop in the region of the Planck mass, and that surviving PBH remnants might explain some or all of the current cold dark matter [11, 12, 13].

Larger PBHs with masses well above $\sim 10^{15}$ g could be observable by means of gravitational effects such as their contribution to the cosmological density parameter [14, 15], gravitational radiation emitted from coalescing binary PBH systems [16] or micro-lensing (PBHs were suggested as possible candidates for some of the objects observed by the MACHO Collaboration [17] and subsequent surveys, although the idea that they might comprise a significant fraction of the halo dark matter is now no longer favoured [18, 19]). All of these aspects have been studied and constraints obtained both on the fraction of matter in the Universe that could now be in the form of PBHs and also on the spectral index of fluctuations on small scales [20, 21, 22, 23, 24].

In this article, we present results from general relativistic numerical simulations of PBH formation in the background of an expanding universe in the radiation-dominated era. There have been a number of previous studies of this type and our aim here is to re-visit the subject area, highlighting some features which we think are important and interesting. A particular aspect of our study is that we use initial perturbations representing growing-mode overdensities with length-scales larger than

the horizon and still within the linear regime. Their evolution is then followed as they subsequently become nonlinear. A convenient parameter for measuring perturbation amplitudes is the fractional mass-excess within the overdense region (denoted by δ); if this is greater than a critical value δ_c (super-critical perturbations), the following nonlinear evolution will result in formation of a black hole, whereas if it is smaller than δ_c (sub-critical perturbations), the overdensity will eventually disperse back into the surrounding medium. Determining the value of δ_c is very important for the cosmological considerations mentioned above.

Following the earliest papers on this subject [2, 3, 4], Carr (1975) [14] carried out a quantitative study based on a simplified model consisting of an overdense collapsing region, described by a closed Friedmann-Robertson-Walker (FRW) spacetime, surrounded by a spatially-flat FRW expanding background. For a radiation-dominated universe, his calculation gave $\delta_c = 1/3$ and the black holes formed had masses M_{BH} of the same order as the horizon mass at the time when the fluctuation first entered the horizon. Nadezhin, Novikov & Polnarev (1978) [25] carried out the first detailed numerical study of PBH formation using a hydrodynamical computer code similar to those of May & White (1966) [26] and Podurets (1964) [27] using a “cosmic-time” coordinate with a diagonal metric which reduces to a form similar to that of the FRW metric in the absence of perturbations. A well-known difficulty with this approach is that in a continuing collapse, singularities typically appear rather quickly and stop the computation before the black hole formation is complete. In [25], this difficulty was overcome by using an early form of excision with the evolution being stopped in the region where the singularity would appear. The qualitative features of the earlier picture were basically confirmed but it was found that the PBH masses were always much smaller than the horizon mass.

Shortly afterwards, Bicknell & Henriksen (1979) [28] carried out related calculations using a method based on integration along hydrodynamical characteristics which avoids the problems associated with the appearance of singularities. They used rather different initial data from that of [25] and found formation of black holes with masses of the same order as the horizon mass (or greater in cases where the overdensity in the initial perturbation was not compensated by a surrounding under-dense region).

They noted the appearance of both ingoing and outgoing compression waves during evolutions leading to black hole formation.

More recently, Niemeyer & Jedamzik [29, 30] made further numerical calculations, particularly focusing on the relevance of scaling-laws for PBH formation. They found that M_{BH} follows a power law in $(\delta - \delta_c)$ when the latter is sufficiently small, which is a similar behaviour to that seen in critical collapse by Choptuik [31] and many subsequent authors (see Evans & Coleman [32] and the review by Gundlach [33]). They started from initial perturbations specified at the moment when the overdensity enters the horizon and then computed the subsequent evolution. They used a null-slicing code, following the formulation by Hernandez & Misner (1966) [34], and obtained $\delta_c \simeq 0.7$ for each of the three types of perturbation profile which they studied.

While Niemeyer & Jedamzik [30] demonstrated the existence of a scaling law for PBH masses down to around one tenth of the horizon mass, they did not investigate smaller masses and so it was not possible to determine whether the scaling law was likely to continue down to vanishingly small masses (when $\delta \rightarrow \delta_c$) as in type II critical collapse. In fact, the calculations become very challenging from a numerical point of view when δ is very close to δ_c because of the appearance of strong shocks and deep voids outside the region where the PBH is forming. Hawke & Stewart (2002) [36] addressed this problem using a sophisticated purpose-built code which allowed them to make calculations for values of δ closer to δ_c and to handle the strong shocks which occur in these cases. They found that the scaling law does *not* continue down to very small values of $(\delta - \delta_c)$ but rather reaches a minimum value for M_{BH} around 10^{-4} of the horizon mass, with the limit resulting from the behaviour of the shocks produced in nearly critical collapse.

Shibata & Sasaki (1999) [37] presented an alternative formalism for studying PBH formation using constant mean curvature time slicing and focusing on metric perturbations rather than density perturbations. They emphasised the importance of using initial data which can be directly related to perturbations arising from inflation. Their formulation was not restricted to spherical symmetry (as had been the case for the previous authors mentioned here) but they presented results only from spherical calculations. They located the threshold perturbation amplitude for

PBH formation (in terms of the metric perturbation) and found that this varied considerably depending on the density of the medium surrounding the density peak. They concluded from this that it is probably important to take into account spatial correlations of density fluctuations when considering PBH formation.

It is not straightforward to make the link between results from this type of calculation and ones from the more standard approach focused on density fluctuations. However, this was addressed in a recent paper by Green et al. (2004) [38]. They calculated the PBH abundance produced from two different fluctuation spectra, using peaks theory together with the threshold criterion of Shibata & Sasaki [37]. They then compared the results of this with ones obtained from a standard calculation based on a Press-Schechter-like approach and using density perturbations. They found that the Shibata & Sasaki results are consistent with ones using a density perturbation if δ_c lies in the range $0.3 \lesssim \delta_c \lesssim 0.5$ and they noted the discrepancy with the results of [30].

As mentioned previously, our aim in the work described in this paper was to re-visit some issues arising from these earlier calculations. In particular, we wanted to check on the scaling laws found in [30] and to investigate the effect on them both of starting the initial perturbations earlier, as pure growing modes within the linear regime, and also of including vacuum energy (as a cosmological constant term). For our calculations, we used a null-slicing code, modified from that of Miller & Motta (1989) [39], which implements an essentially identical method to that used in [30] (but with one key technical difference which we discuss in Section 2). This is not as sophisticated in its treatment of the hydrodynamics as the Hawke & Stewart code [36] but is satisfactory for our purposes and has some useful advantages particularly as regards the specification of initial conditions. We have examined both supercritical and sub-critical perturbations. The most notable results are: *(i)* we find good agreement with the results of [30] when we use the same initial data; *(ii)* we obtain $\delta_c \simeq 0.45$ when we use initial data specified as purely growing-mode perturbations, consistent with the results of Green et al. [38]; *(iii)* when a cosmological constant term Λ is included, δ_c increases linearly with increasing Λ ; *(iv)* subcritical collapse with δ sufficiently close to δ_c produces strong compressions and rarefactions before the overdensity subsides back into the surrounding medium.

The organisation of the paper is as follows. In Section 2, we review the mathematical formulation of the problem and the calculation method used; Section 3 presents results from our calculations of PBH formation and sub-critical collapse; Section 4 contains discussion and conclusions. We use units for which $c = G = 1$ except where otherwise stated.

2. Mathematical formulation & calculation method

For our calculations we have followed a procedure very similar to that of Niemeyer & Jedamzik [30]. We will not repeat their full discussion of the method but nevertheless it can be useful to make some further comments about it here.

As with most of the other literature on this subject, we are restricting attention to spherical symmetry, which very greatly simplifies the calculations, and we have used the formulations of the relativistic hydrodynamical equations given by Misner & Sharp (1964) [40] and Hernandez & Misner (1966) [34]. Both of these are Lagrangian formulations, the first using a diagonal metric (with the time referred to as “cosmic time” which reduces to the familiar FRW time coordinate in the absence of perturbations), and the second using an outward null slicing where the time coordinate is an “observer time” (the clock time as measured by a distant fundamental observer). The cosmic-time formulation is particularly simple and has the advantage of using a slicing which many people find intuitive; this was the approach used by May & White (1966) [26] in their classic paper studying spherically-symmetric gravitational collapse. However, as mentioned above, this approach has a well-known drawback for studying black hole formation in that singularities are typically formed rather early in calculations of continuing collapse and it is not then possible to follow the subsequent evolution. The outward null slicing approach is particularly convenient for calculations involving black hole formation in spherical symmetry: anything which could not be seen by a distant observer (e.g. singularity formation) does not occur within the coordinate timespan, while all observable behaviour can be calculated. This is, in some sense, the optimal approach for studying black hole formation in spherical symmetry as seen by an outside observer (being linked directly to potential observations) although

more sophisticated slicing conditions have advantages for calculations away from spherical symmetry.

Following the introduction of the observer-time approach by Hernandez & Misner in 1966 [34], it was implemented soon afterwards in unpublished calculations. A brief presentation of some results was given by Miller & Sciama (1980) [41] and a full discussion of the technique used and of results obtained was given subsequently by Miller & Motta (1989) [39]. A problem with the use of this method concerns the satisfactory specification of initial conditions which is not natural to do on a null slice. Because of this, Miller & Motta [39] made a preliminary calculation using the Misner & Sharp [40] formulation in order to construct data on an outgoing null slice from initial conditions specified on a space-like slice; the observer-time calculation then proceeded from the null-slice data constructed in this way. Subsequently, Baumgarte, Shapiro & Teukolsky (1995) [42] made calculations using a similar technique and it was these which were used as a reference point by Niemeyer & Jedamzik [30].

For the calculations of PBH formation reported in this paper, we have used a modification of the Miller & Motta code [39] (designed for studying the collapse of an isolated object surrounded by vacuum) together with elements from the codes by Miller & Pantano (1990) [43] and Miller & Rezzolla (1995) [44] (designed for following phase-transition bubble growth within an expanding universe).

In the remainder of this section, we give a brief overview of the equations used and of our numerical code. The reader is referred to the papers quoted above for further details.

2.1. The Misner-Sharp equations

For calculations in spherical symmetry, it is convenient to divide the collapsing matter into a system of concentric spherical shells and to label each shell with a Lagrangian co-moving radial coordinate which we will denote with r . The metric can then be written in the form

$$ds^2 = -a^2 dt^2 + b^2 dr^2 + R^2 (d\theta^2 + \sin^2 \theta d\varphi^2), \quad (1)$$

where R (the Schwarzschild circumference coordinate), a and b are functions of r and the time coordinate t . This was the form used Misner & Sharp (1966) [40].

For a classical fluid, composed of particles with nonzero rest-mass, it is convenient to use the rest-mass μ contained interior to the surface of a shell (or, equivalently, the baryon number) as its co-moving coordinate r . For the case of a radiation fluid (as studied in this paper), rest-mass and baryon number are not available as conserved quantities to be used in this way but a similar procedure can still be followed by introducing the concept of a conserved number of unit co-moving fluid elements (Miller & Pantano 1990) [43]. Denoting a “relative compression factor” for these fluid elements by ρ (equivalent to the rest-mass density in the standard treatment), one then has

$$d\mu = 4\pi\rho R^2 b dr, \quad (2)$$

and identifying μ and r then gives

$$b = \frac{1}{4\pi R^2 \rho}. \quad (3)$$

Following the notation of [40], we write the equations in terms of the operators

$$D_t \equiv \frac{1}{a} \left(\frac{\partial}{\partial t} \right), \quad (4)$$

$$D_r \equiv \frac{1}{b} \left(\frac{\partial}{\partial \mu} \right), \quad (5)$$

and applying these to R gives

$$D_t R \equiv U, \quad (6)$$

$$D_r R \equiv \Gamma, \quad (7)$$

where U is the radial component of the four-velocity in the associated Eulerian frame, using R as the radial coordinate, and Γ is a generalisation of the Lorentz factor.

We are mostly dealing with processes occurring in the radiation dominated era of the Universe for which the equation of state of the matter can be written as

$$p = \frac{1}{3} e, \quad (8)$$

where p is the pressure and e is the energy density. For one-parameter equations of state of the form $p = p(e)$, the system of Einstein and hydrodynamic equations can then be written as:

$$D_t U = - \left[\frac{\Gamma}{(e+p)} D_r p + \frac{M}{R^2} + 4\pi R p \right], \quad (9)$$

$$D_t \rho = -\frac{\rho}{\Gamma R^2} D_r (R^2 U), \quad (10)$$

$$D_t e = \frac{e+p}{\rho} D_t \rho, \quad (11)$$

$$D_r a = -\frac{a}{e+p} D_r p, \quad (12)$$

$$D_r M = 4\pi \Gamma e R^2, \quad (13)$$

where M is a measure of the mass-energy contained inside radius μ and Γ can be calculated either from (7) or from the constraint equation

$$\Gamma^2 = 1 + U^2 - \frac{2M}{R}. \quad (14)$$

2.2. The Hernandez-Misner Equations

Because of the problems mentioned earlier, Hernandez & Misner [34] introduced the concept of “observer time”, using as the time coordinate the time at which an outgoing radial light ray emanating from an event reaches a distant observer[‡]. In the original formulation, this observer was placed at future null infinity but for calculations in an expanding cosmological background we use an FRW fundamental observer sufficiently far from the perturbed region to be unaffected by the perturbation. Along an outgoing radial null ray we have

$$a dt = b dr, \quad (15)$$

and we define the observer time u by

$$f du = a dt - b dr, \quad (16)$$

with f being an integrating factor which needs to be determined. In terms of this, the metric becomes

$$ds^2 = -f^2 du^2 - 2fb dr du + R^2 (d\theta^2 + \sin^2 \theta d\varphi^2), \quad (17)$$

which is no longer diagonal. The operators equivalent to (4) and (5) are now

$$D_t \equiv \frac{1}{f} \left(\frac{\partial}{\partial u} \right), \quad (18)$$

$$D_k \equiv \frac{1}{b} \left(\frac{\partial}{\partial r} \right) = 4\pi \rho R^2 \left(\frac{\partial}{\partial \mu} \right), \quad (19)$$

[‡] We note that a somewhat similar approach, but based on a double null foliation, has recently been used by Harada et al. [35] for studying some different aspects of PBH formation.

where D_k is the radial derivative across the null slice and the corresponding derivative across the Misner-Sharp space-like slice is given by

$$D_r = D_k - D_t. \quad (20)$$

The observer-time equations replacing the cosmic-time ones (9) – (13) are then:

$$D_t U = -\frac{1}{1 - c_s^2} \left[\frac{\Gamma}{(e + p)} D_k p + \frac{M}{R^2} + 4\pi R p + c_s^2 \left(D_k U + \frac{2U\Gamma}{R} \right) \right], \quad (21)$$

$$D_t \rho = \frac{\rho}{\Gamma} \left[D_t U - D_k U - \frac{2U\Gamma}{R} \right], \quad (22)$$

$$D_t e = \left(\frac{e + p}{\rho} \right) D_t \rho, \quad (23)$$

$$D_k f = \frac{f}{\Gamma} \left(D_k U + \frac{M}{R^2} + 4\pi R p \right), \quad (24)$$

$$D_k M = 4\pi R^2 [e\Gamma - pU], \quad (25)$$

where $c_s = \sqrt{(\partial p / \partial e)}$ is the sound speed, which is equal to $1/\sqrt{3}$ in the present case.

The quantity Γ is given by equation (14), as before, and also by

$$\Gamma = D_k R - U. \quad (26)$$

Using equations (24), (25) and (14), it is possible to derive the following alternative equation for f :

$$D_k \left[\frac{(\Gamma + U)}{f} \right] = -4\pi R (e + p) f. \quad (27)$$

In calculations concerning collapse of an isolated object surrounded by vacuum in an asymptotically-flat spacetime, the observer time is taken to be the clock time of a static observer at future null infinity and so $(\Gamma + U)/f = 1$ at the location of that observer (since $\Gamma = 1$, $U = 0$ and $f = 1$ there). It then follows from equation (27) that $(\Gamma + U)/f = 1$ also at the surface of the collapsing object, since the right hand side of (27) is zero in vacuum. The condition

$$f = \Gamma + U, \quad (28)$$

at the surface is used as a boundary condition for f and the values of f internal to that are then calculated from equation (24).

The general condition for a trapped surface is $D_k R \leq 0$. With outgoing null slicing, $D_k R = 0$ should be reached only asymptotically in the future, accompanied by the lapse f going to zero, and $D_k R$ should never become negative. In practice, care is required in order to achieve the exact synchronization of $D_k R \rightarrow 0$ and $f \rightarrow 0$ in a numerical solution where the equations are discretized; if the synchronization is not achieved, negative values of $D_k R$ do appear and the evolution becomes unphysical.

In the case of an isolated collapsing object surrounded by vacuum, using boundary condition (28) together with equation (24) ensures the correct behaviour. However, for the present situation, where the surroundings are not vacuum and the spacetime is not asymptotically flat, it is necessary to proceed in a different way. We are wanting to synchronise the “observer time” with the clock time of a co-moving FRW fundamental observer at the outer edge of the grid (setting $f = 1$ there) and then to calculate f elsewhere using this as a boundary condition. For doing this, we found it essential to use equation (27), which guarantees synchronisation of $D_k R \rightarrow 0$ and $f \rightarrow 0$, rather than equation (24), which always eventually gave rise to unphysical behaviour with $D_k R < 0$. We think that this is a crucial point in using an outward null slicing technique for any situation regarding black hole formation within non-vacuum surroundings. It will apply equally to calculations of black hole formation from core-collapse of high-mass stars.

2.3. The calculation method

As mentioned above, our calculations of PBH formation have been made using an explicit Lagrangian hydrodynamics code based on that of Miller & Motta (1989) [39] but with the grid organised in a way similar to that in the code of Miller & Rezzolla (1995) [41], which was designed for calculations in an expanding cosmological background. The reader is referred to those papers for full details of the methods used and we repeat just some main points here. The method described by Niemeyer & Jedamzik [30], following from the Baumgarte et al. code [42], is similar in most respects. In order to achieve good grid coverage, we have used a composite prescription for the grid spacing, with $\Delta\mu$ increasing exponentially going outwards through the inner and outer parts of the grid but remaining constant in the intermediate region.

We start our perturbations in the linear regime with length-scales larger than the cosmological horizon radius R_H , and have the grid reaching out to $10 R_H$ with around 2000 grid points.

For collapses leading to black hole formation, our calculations proceed in two stages: first, initial data is specified on a space-like slice at constant cosmic time, specifying the energy density e and the four-velocity component U as functions of R at an initial time t_i . This data is then evolved using the Misner-Sharp equations of Section 2.1 so as to generate a second set of initial data on a null slice (at constant observer time). To do this, an outgoing radial light ray is traced out from the centre and parameter values are noted as it passes the boundary of each grid zone. The second set of initial data, constructed in this way, is then evolved using the Hernandez-Misner equations of Section 2.2. For sub-critical cases, which end eventually with dispersal of the perturbation into the surrounding uniform medium, we have continued with the Misner-Sharp cosmic-time approach throughout.

The unperturbed background model is taken as a spatially-flat FRW model, for which $\Gamma = 1$ (giving $U = \sqrt{2M/R}$) with $e(r) = \text{constant}$ at any particular cosmic time t . The perturbations of e and U are then superimposed on this background in the way described in the next section. During the following evolutions, the metric functions a (for cosmic time) and f (for observer time) are set equal to unity at the outer boundary of the grid, thus synchronising the cosmic and observer times with local clock time there as measured by the local co-moving FRW fundamental observer.

3. Description of the calculations

In this section, we describe our calculations for both super-critical and sub-critical perturbations.

3.1. Initial Conditions

As initial conditions for our calculations, we use spherically symmetric density perturbations superimposed on a uniform FRW background. The perturbations are

specified in terms of the dimensionless quantity

$$\delta_e(R) \equiv \frac{e - e_b}{e_b}, \quad (29)$$

where e_b is the uniform background density given by $e_b = 3/32\pi t$ at any particular time t . Niemeyer & Jedamzik [30] used three different types of expression for δ_e (shown in Figure 1 of their paper):

Gaussian:

$$\delta_e(R) = A \exp\left(-\frac{2R^2}{(LR_H)^2}\right), \quad (30)$$

Mexican hat:

$$\delta_e(R) = A \left(1 - \frac{R^2}{L^2 R_H^2}\right) \exp\left(-\frac{3R^2}{2L^2 R_H^2}\right), \quad (31)$$

Polynomial:

$$\delta_e(R) = \begin{cases} \frac{A}{9} \left(1 - \frac{R^2}{L^2 R_H^2}\right) \left(3 - \frac{R^2}{L^2 R_H^2}\right) & \text{if } R < \sqrt{3}(LR_H) \\ 0 & \text{if } R \geq \sqrt{3}(LR_H) \end{cases} \quad (32)$$

where the parameters A and L set the amplitude and length-scale of the perturbation. For the Mexican-hat and polynomial perturbations, the excess energy in the overdense region is exactly balanced by the deficit in the outer underdense region (i.e. $\int_0^\infty 4\pi\delta_e R^2 dR = 0$), whereas the Gaussian ones have only an excess, decreasing asymptotically to the background value. The latter is not very satisfactory for cosmological perturbations and so we concentrate here on the first two types.

We follow the previous literature in also using an “integrated” perturbation δ which represents the mass-energy excess in the overdense region with respect to that in a corresponding uniform solution:

$$\delta \equiv \frac{\int_0^{R_o} 4\pi\delta_e R^2 dR}{\frac{4}{3}\pi R_o^3}, \quad (33)$$

where R_o is the radius of the overdensity. (In the case of the Gaussian, R_o is defined as the radius at which δ_e has fallen to $1/e^2$ of its value at $R = 0$.)

We are mostly starting with perturbations which are still on length-scales much larger than the horizon scale [$R_o/R_H \geq 5$] and are well within the linear regime

[typically $\delta \sim 10^{-2}$]. Setting initial conditions within the linear regime makes it easy to specify consistent density and velocity perturbations representing a purely growing mode: δ_e grows linearly with time and the associated velocity perturbation is given roughly by

$$\delta_u(R) = -\frac{\delta_e}{4}, \quad (34)$$

(coming from formulae in [45]), where δ_u is defined in the same way as for δ_e in equation (29):

$$\delta_u(R) \equiv \frac{U - U_b}{U_b}, \quad (35)$$

with $U_b(R) = HR$ being the velocity field of the background Hubble flow. (We are here considering adiabatic perturbations with a Newtonian gauge, in which the perturbations do not generate off-diagonal components of the metric.) The corresponding decaying modes have decreasing amplitudes and, if excited by some process, would disappear again rather rapidly. Of the perturbations produced from inflation, only growing modes are of interest at the times which we are considering here.

3.2. Evolution of supercritical perturbations

In this sub-section, we describe results from representative evolutions leading to black hole formation, carried out using the null-slicing formulation.

Before moving on to new calculations, we first needed to check on whether our code did reproduce the results of Niemeyer & Jedamzik [30] when we used their choice of initial conditions and a simple exponential grid similar to theirs. We found extremely close agreement. For perturbations with the initial δ only slightly larger than the critical value δ_c , the masses of the black holes produced, M_{BH} , follow a scaling law:

$$M_{BH} = K(\delta - \delta_c)^\gamma M_H(t_H), \quad (36)$$

where K and γ are constants and $M_H(t_H)$ is the cosmological horizon mass at the horizon-crossing time t_H (i.e. when $R_o(t_H) = R_H(t_H)$). The type of behaviour given by (36) is familiar from the literature on critical collapse (which, however, is generally

considering collapse under simpler circumstances and not within the context of an expanding universe). Our results match very closely with those of [30], with $\delta_c \simeq 0.67$ for the Mexican-hat profile and $\simeq 0.71$ for the polynomial and Gaussian profiles and with γ between $0.36 - 0.37$ in each case. These values for γ are very close to the value $0.356\dots$ calculated semi-analytically for the same equation of state within the standard critical collapse scenario [46].

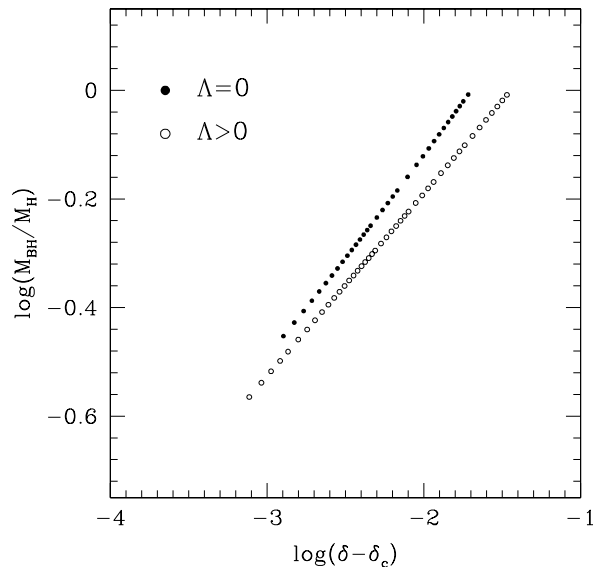


Figure 1. Scaling behaviour for M_{BH} as a function of $(\delta - \delta_c)$ calculated for growing-mode Mexican-hat perturbations specified within the linear regime. The filled circles refer to the standard calculation discussed in section 3.2, while the open circles are for a calculation including a non-zero cosmological constant Λ , as discussed in section 3.3, giving $y = 3.0 \times 10^{-3}$.

Following these initial calculations to reproduce previous results, we then carried out further ones starting from growing-mode perturbations specified within the linear regime and with length-scales larger than the cosmological horizon. These perturbations were evolved with the Misner-Sharp code until the moment when they entered the horizon and the current value of δ was then calculated for use as our measure of perturbation amplitude in the discussion of scaling laws. Having done this, we switched to the Hernandez-Misner code for completing the calculation.

Plotting the eventual black hole mass against $(\delta - \delta_c)$, we obtained scaling curves very similar to those of [30] (and with almost identical values of γ) but with substantially different values for δ_c : for Mexican-hat perturbations, we found $\delta_c \simeq 0.43$ and for polynomial perturbations, $\delta_c \simeq 0.47$. Our scaling-law results for Mexican-hat perturbations are shown as the $\Lambda = 0$ curve in Figure 1. The reason for the changed values of δ_c is clear: in [30] the initial perturbations, specified at the horizon-crossing time, had part of their amplitude contributed by a decaying-mode component which then rapidly decreased leaving only the growing-mode part visible. Only the part of the perturbation amplitude corresponding to the growing mode is relevant for the black hole formation and so the effective δ is smaller than that calculated in [30].

Noting the work of Hawke & Stewart (2002) [36] and the fact that the horizon-scale is an important length-scale in the problem, we do not expect that the linear scaling law will continue to indefinitely small values of M_{BH} and $(\delta - \delta_c)$ but, instead, that it will level off at some minimum value of M_{BH} . Confirming this behaviour in the case of growing-mode perturbations starting in the linear regime is of great interest but would require refinement of our present code to increase resolution and improve the capacity for handling strong shocks.

Figure 2 shows some more detailed results for a particular representative case within the linear scaling regime. This run starts from a growing-mode Mexican-hat perturbation with $R_o/R_H = 5$ giving $(\delta - \delta_c) = 2.37 \times 10^{-3}$ at horizon crossing, which leads to formation of a black hole with $M_{BH} = 0.4415 M_H(t_H)$. The top two panels show the evolution of the lapse f and the corresponding behaviour of the fluid worldlines. The interpretation of the collapse of the lapse is particularly clear when an observer-time formulation is used: as $f \rightarrow 0$, the redshift of outgoing signals increases and the evolution as seen by a distant observer becomes frozen, corresponding to black hole formation (see also the small inset where $\log f$ is plotted). Note, however, that strictly “black hole formation” occurs only asymptotically in the future according to this formulation. In the plot for the worldlines, one can see the separation between the matter which goes to form the black hole and the matter which continues to expand, with a semi-evacuated region being formed between them. Note that some of the outer material first decelerates but then accelerates again before

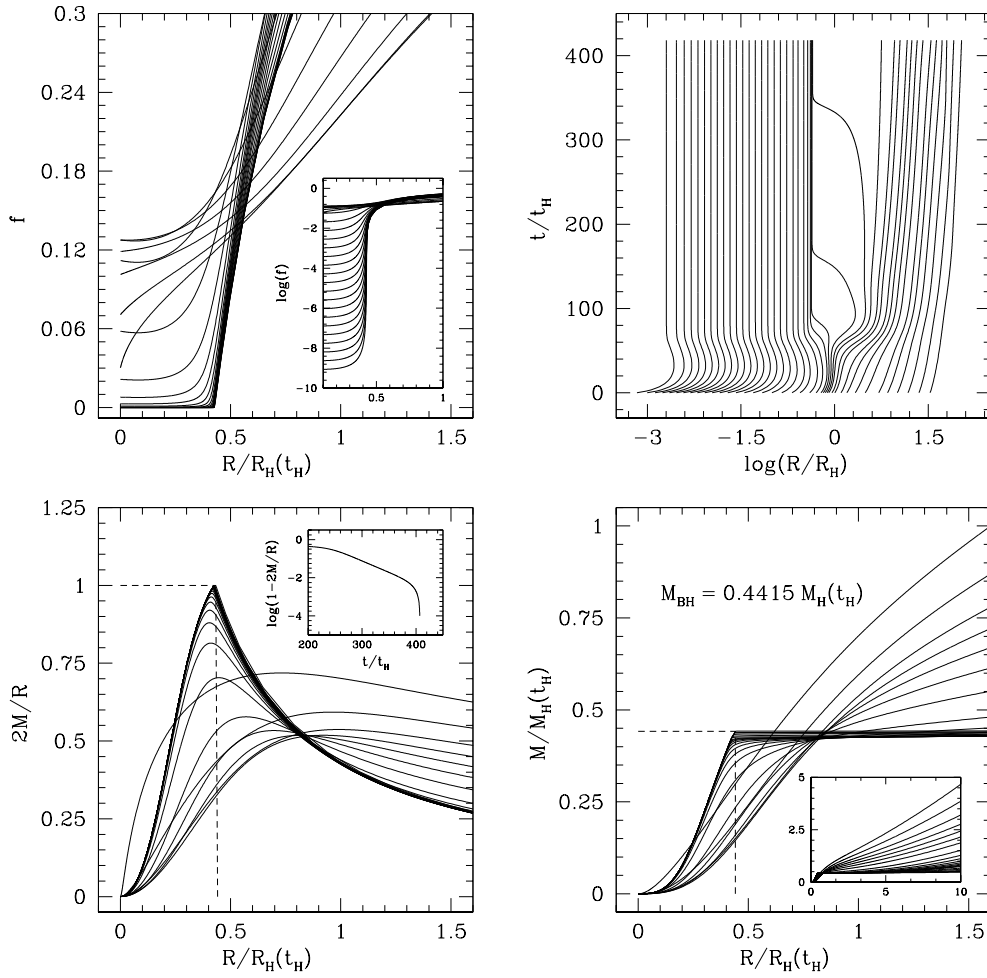


Figure 2. A typical evolution leading to black hole formation: the initial perturbation had a Mexican-hat profile and gave $(\delta - \delta_c) = 2.37 \times 10^{-3}$ at the horizon crossing time. The top left-hand panel shows the behaviour of the lapse function (the time sequence of the curves goes from bottom to top on the right hand side); the top right-hand panel shows the fluid-element worldlines (the time is measured in units of the horizon-crossing time t_H). The bottom left-hand panel shows the profile of $2M/R$ at different times, with the inset showing the approach of the maximum value of $2M/R \rightarrow 1$; the bottom right-hand panel shows the corresponding evolution of the mass-energy (in both of these panels, the time sequence of the curves goes from top to bottom on the right hand side).

crossing this semi-evacuated region to fall onto the black hole. The bottom left-hand panel of Fig. 2 shows the behaviour of the ratio $2M/R$, plotted against R at successive times. The event horizon corresponds to the asymptotic location of the outermost trapped surface, where $D_k R = 0$ and $R = 2M$. For the present purposes, we need an operational definition for calculating M_{BH} , bearing in mind that the black hole is only formed asymptotically and that further material may continue to accrete. The inset in the bottom left-hand panel of Fig. 2 shows the approach of the maximum value of $2M/R \rightarrow 1$: our operational definition for M_{BH} is to set it equal to the value of M at the maximum of $2M/R$ when $(1 - 2M/R)$ first becomes smaller than 10^{-4} . The bottom right-hand panel shows a corresponding plot for M against R . It can be seen that the profiles for M become very flat just outside the black hole region at late times, a consequence of the very low densities being reached there (less than 10^{-4} of the background density at the horizon-crossing time). The small inset shows the continuation of this figure up to larger radial scales. For calculations with δ closer to δ_c , the rarefactions formed become increasingly deep, and one sees strong shock waves appearing at the outer edge of the under-dense region.

3.3. Evolution of super-critical perturbations when $\Lambda > 0$

We were also interested to investigate the effect for PBH formation of including a cosmological constant large enough to affect the dynamics. We recognise that this is a highly idealised scenario since the present-day cosmological constant would have had negligible effect in the early universe and other vacuum energies present after inflation are unlikely to have been constant in time (e.g. quintessence). However, it is of conceptual interest to find out what the behaviour would be in this hypothetical case. A cosmological constant Λ is equivalent to a false vacuum with energy density $e_v = \Lambda/8\pi$ and pressure $p_v = -\Lambda/8\pi$. Its effect can be included by adding these terms onto the standard energy density e and pressure p wherever those appear.

A positive Λ eventually causes the expansion of the universe as a whole to start accelerating and acts against the growth of overdensities, while a negative Λ would aid general collapse. (The equations governing the background expansion when $\Lambda \neq 0$ are summarised in the Appendix.) As the background density decreases with time, the

cosmological constant becomes progressively more important until, when e_v becomes greater than e , the deceleration is reversed and becomes an acceleration [see equation (A.2)]. It is convenient to introduce a quantity y , the ratio between the vacuum energy and the total energy in the uniform background

$$y \equiv \frac{e_v}{e + e_v}, \quad (37)$$

which can then be written as

$$y = \frac{4}{3}\Lambda M_H^2, \quad (38)$$

since $M_H = \frac{4}{3}\pi R_H^3(e + e_v)$ with $R_H = 2M_H$ (Note that this type of relation holds for the cosmological horizon in the same way as for a black hole event horizon)[§]. In the following, we will use y as a general measure of the importance of the Λ term, with M_H being measured at the horizon-crossing time for a perturbation with $\delta = \delta_c$. The influence of Λ during formation of a black hole of mass M_{BH} can similarly be characterised by the quantity ΛM_{BH}^2 and so, for a given Λ , is greatest for large black holes.

In making computations with $\Lambda > 0$, it is particularly important to start the calculation at an early time when the perturbation has a length-scale larger than the horizon. For appreciating its effects, one wants Λ to be sufficiently large so as to make a significant difference for the collapse, but not so large that it creates a problem for constructing the null-slice initial data. By starting the calculation sufficiently early, this can be achieved although the values of y which we will be considering are all very small (in the range $10^{-3} - 10^{-2}$).

The qualitative picture of collapses leading to black hole formation is not changed very greatly by the presence of a Λ term but there are significant differences in the parameters of the scaling law. We started all of these calculations with perturbations at five times the horizon scale (i.e. $R_o/R_H = 5$).

The impact of Λ on the scaling law can be seen in Figure 1: γ decreases for $\Lambda > 0$ and for sufficiently small Λ is found to follow a linear relationship

$$\gamma(\Lambda) \simeq \gamma(0) - 8.3y. \quad (39)$$

[§] Both are trapped surfaces. A black hole event horizon is the asymptotic location of the outermost trapped surface for outgoing light-rays whereas the cosmological horizon is the innermost trapped surface for incoming light rays.

The critical amplitude δ_c increases with increasing Λ and also follows a linear relationship:

$$\delta_c(\Lambda) \simeq \delta_c(0) + 0.98 y. \quad (40)$$

This behaviour can be interpreted as follows: a positive Λ acts against collapse, so that corresponding black hole masses will be lower and the threshold amplitude δ_c will be raised. For a given Λ , its influence is greater for larger black-hole masses than for smaller ones ($\propto M_{BH}^2$) and this gives rise to the observed decrease in γ .

3.4. Evolution of subcritical perturbations

For subcritical perturbations with δ considerably less than δ_c , the perturbation initially grows but then subsides back into the surrounding medium in an uneventful way. However, for perturbations with δ sufficiently close to δ_c , some very interesting behaviour is seen and we present results from a representative case of this in the present subsection. Our calculations for subcritical perturbations use only the Misner-Sharp code.

The run presented starts with a Mexican-hat perturbation specified in the linear regime, with $(\delta - \delta_c = -3 \times 10^{-3})$. In Figure 3, the fluid worldlines are plotted and the main features of interest can already be seen from this. Figures 4 and 5 then show details of the evolution of the energy density e and the radial velocity U . Figure 4 shows a sequence of snap-shots of these quantities, plotted as a functions of R , at key moments during the evolution. Figure 5 shows the time evolution of these quantities at three (comoving) locations: near the centre of the perturbation, at an intermediate region (mid-way through the collapsing matter) and at the edge of the grid where the fluid is unperturbed.

The evolution can be summarized in terms of the following steps (see particularly Figures 3 and 4):

- (i) Initially, the perturbation has very small amplitude ($\delta_e \sim 10^{-2}$) and its length-scale is five times the horizon scale; the perturbation amplitude then grows within the expanding fluid. The deceleration in the perturbed region is larger than that in the unperturbed region and its expansion lags progressively behind that of

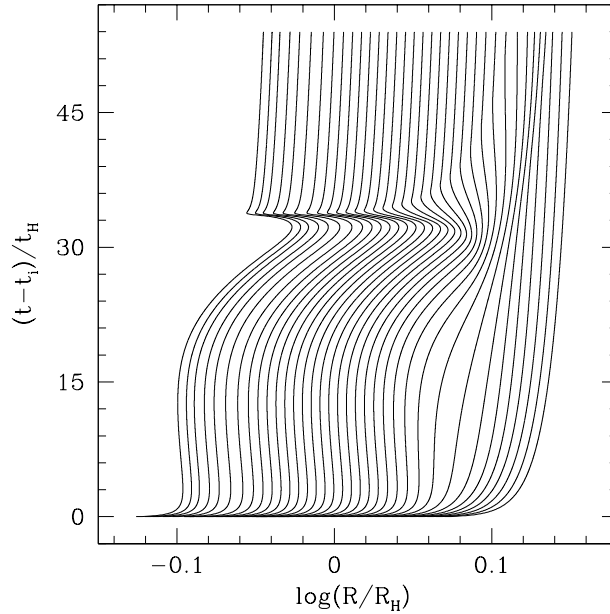


Figure 3. Worldlines for a Mexican-hat perturbation with $(\delta - \delta_c) = -3.0 \times 10^{-3}$. This plot shows alternating collapse and expansion of the perturbed region while the outer material continues to expand uniformly. The “cosmic” time is measured in units of the time at horizon crossing.

the outer matter until eventually it starts to re-contract shortly after horizon crossing. The maximum infall velocity reached is, however, rather small [see row (a) of Figure 4 which is for a time considerably after horizon crossing, when the perturbation has become very nonlinear]. The infall can be clearly seen in Figures 3 and 4 but is only just visible in the second frame of Figure 5.

- (ii) The contraction is not strong enough to produce a black hole and the fluid bounces out again [row (b)], expanding until it encounters the surrounding matter which did not participate in the contraction. A compression wave forms where the two regions of fluid meet, while the density becomes very low at the centre of the perturbation [row (c)].
- (iii) The compression wave proceeds out into the surrounding material [row (d)] but also some matter is sent back into the middle of the rarefaction where it

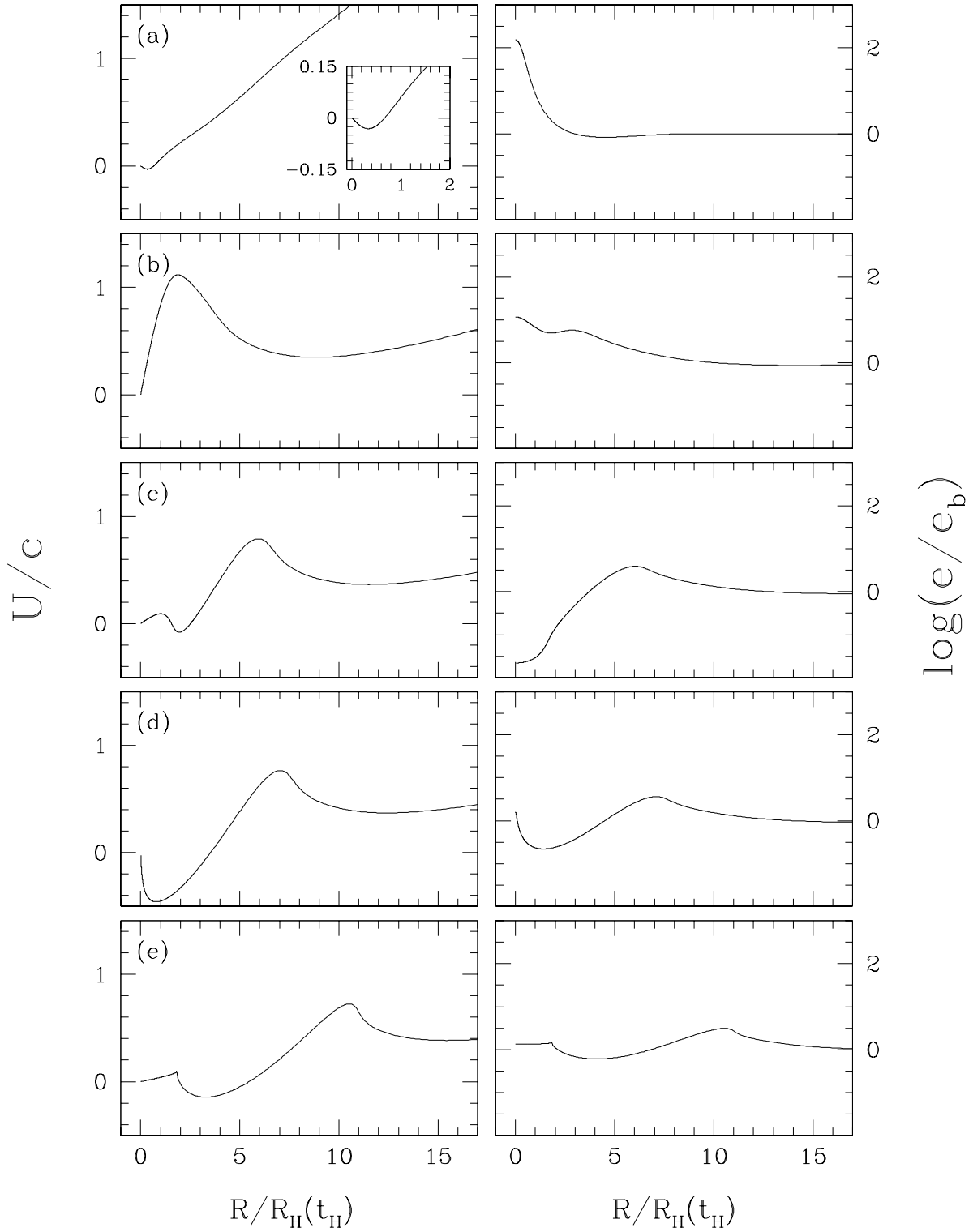


Figure 4. Plots of local quantities as functions of $R/R_H(t_H)$: the velocity U/c is shown in the left-hand column and the energy density e/e_b in the right-hand column. The frames correspond to the following values of $(t-t_0)/t_H$: (a) 7.02; (b) 25.92, (c) 31.67; (d) 33.64; (e) 40.11. Note that R_H is increasing with time and so points with $R/R_H(t_H) > 1$ can be within the current horizon scale at times after horizon-crossing.

undergoes a second bounce which is much more extreme than the first with a very abrupt change of velocity in the central regions (as can be seen from Figure 5). Whereas the outward moving compression is damped geometrically as it proceeds to spherical surfaces with progressively larger areas, the inward-moving wave of material is geometrically amplified by the inverse process. The reason for the second collapse and bounce being more violent than the first is that while the first is a collapse of an overdensity which is resisted throughout by internal pressure, the second is essentially the collapse of a “shell” with near vacuum inside it and is hence close to free-fall until just before the bounce.

- (iv) The compression wave formed by the second bounce propagates out into the surrounding medium following the first one [row (e)]. Both proceed to damp geometrically and eventually the medium returns to a uniform state. Note that the second compression wave is very steep fronted (see Figure 4) but is not quite a shock. It is likely that that genuine shocks would be seen for perturbations with δ closer to δ_c .

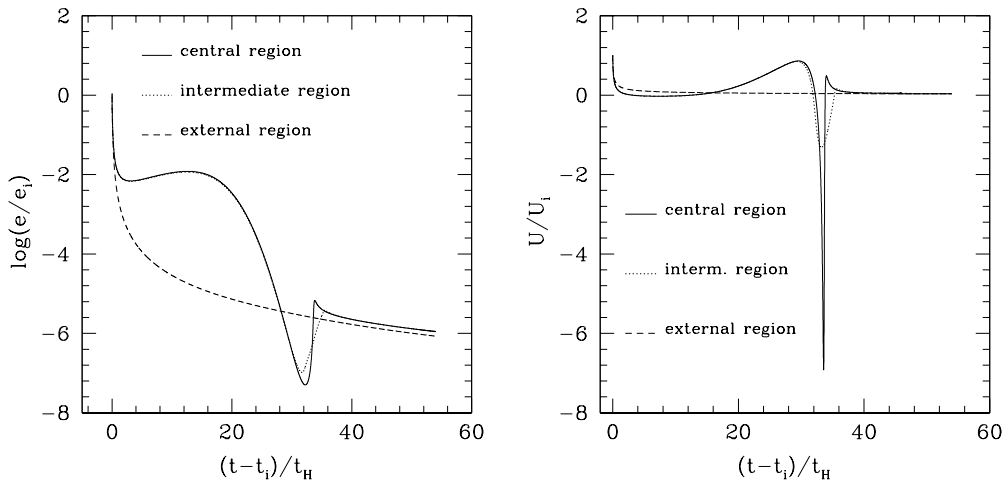


Figure 5. Evolution of the energy density e and radial velocity U at three (comoving) locations: near to the centre of the perturbation, at an intermediate region and at the edge of the grid where the fluid is unperturbed. Each quantity is measured in units of its initial value at the same comoving location.

It is useful to make some further comments about the plots in Figure 5. The left-hand plot shows the density normalized to its initial value at the same comoving location: this shows the variation of the local density against the background of the general decrease in density as the universe expands and allows one to see clearly the local contraction and expansion of the fluid. Initially, the perturbed region is also still expanding but it then starts to contract when the perturbation amplitude has reached a high enough value. The right-hand plot shows the local value of the radial velocity also normalized to its initial value at the same co-moving location. This has a very different behaviour from that of the energy density, with the inward velocity during the second collapse being very much greater than that during the first and the second bounce being far more abrupt. We see just two bounces in our calculation: after this the expansion of the universe prevents further ones, although we expect that more bounces would be seen for an initial perturbation with δ closer to δ_c .

4. Conclusions

We have presented results from calculations of PBH formation in an expanding universe during the radiation dominated era, following a broadly similar approach to that used by Niemeyer & Jedamzik [30] in previous investigations of this subject but with a number of key differences. Growing-mode perturbations were introduced into an otherwise uniform expanding medium and their subsequent behaviour was then followed. Those overdensities with amplitudes δ greater than the critical value δ_c give rise to black hole formation whereas smaller ones contract to a maximum compression and then bounce, eventually dispersing into the surrounding medium. Defining δ to be the fractional mass excess within the overdensity at the time of horizon crossing, we find that δ_c ranges between 0.43 and 0.47, depending on the perturbation shape. These values are consistent with the results of Shibata & Sasaki [37], obtained with a different method, resolving a previously noted discrepancy [38]. We have verified the results of [30] concerning the scaling law relation between the black-hole mass M_{BH} and $(\delta - \delta_c)$ when the latter is sufficiently small. The power of the scaling law γ is essentially unchanged for our modified initial conditions, in contrast with

the large changes seen for δ_c . We note, however, the important results of Hawke & Stewart (2002) [36] who found that, for a class of perturbations specified in a non-linear regime at sub-horizon scales, the scaling law does not continue to arbitrarily small M_{BH} but levels off at around 10^{-4} of the horizon mass due to interaction with the surrounding medium. Our code does not yet have the capability of approaching sufficiently close to δ_c to reveal this effect; it would be important for future work to establish to what extent the Hawke & Stewart [36] result is dependent on the form of the initial conditions.

We have investigated the effect on the scaling law of introducing a cosmological constant term Λ and found that positive values of Λ give rise to lower values of γ and higher values of δ_c , each varying linearly with Λ when the latter is sufficiently small. This can be understood in terms of the effect of a cosmological constant in opposing collapse.

We also studied sub-critical collapses (with $\delta < \delta_c$). When δ is close to δ_c , we find that this can be a surprisingly violent process. The initial collapse and bounce are rather mild, being moderated by the internal pressure, but after the subsequent reflection from the surrounding medium and re-collapse (with matter falling into near-vacuum), the second bounce can be very violent with a rapid velocity change and the sending out of a second compression wave into the surrounding medium following the one produced by the first bounce. After this, the possibility of further bounces is stopped by the overall background expansion for the cases studied (although additional bounces are expected for δ closer to δ_c).

There are a number of topics concerning PBH formation which may be of great interest for cosmology and which we are intending to study further, including: determination of the proportion of the matter in the universe going into black holes according to various scenarios for the perturbations coming from inflation (with the possibility of ruling out some scenarios); investigation of possible enhanced PBH formation at the time of phase transitions (see Jedamzik & Niemeyer [47]); alternative possibilities for the formation of intermediate mass black holes or of the seeds for super-massive black holes at the centres of galaxies (as mentioned by Bicknell & Henriksen [28] in 1979). Work is now in progress to investigate these.

Acknowledgements: In the course of this work, we have benefited from helpful discussions with many colleagues including Bernard Carr, Alexander Polnarev, Marco Bruni, Karsten Jedamzik, Ian Hawke and Carlo Baccigalupi.

Appendix A. Cosmological solution with non-zero Λ

We present here some of the analytic expressions describing an expanding universe with $\Lambda \neq 0$ in the radiation-dominated era. These equations are certainly not being presented here for the first time but they are not easy to find in the usual cosmology textbooks and we think that it may be useful to present them together here. In this part only, we use physical units and do not set $c = G = 1$.

First, we note the forms taken by the Friedman equation and the associated acceleration equation (we are taking the spatially flat case):

$$\left(\frac{\dot{a}}{a}\right) = \frac{8\pi G}{3c^2}e + \frac{\Lambda c^2}{3}, \quad (\text{A.1})$$

$$\left(\frac{\ddot{a}}{a}\right) = -\frac{8\pi G}{3c^2}\left(e - \frac{\Lambda c^4}{8\pi G}\right), \quad (\text{A.2})$$

where e is the energy density of radiation which scales as

$$e = e_i \left(\frac{a_i}{a}\right)^4, \quad (\text{A.3})$$

(here the subscript i refers to a fiducial initial time). Inserting this into (A.1), we obtain the integral equation

$$\int_0^{(a_i/a)} \frac{\frac{a_i}{a'} d\left(\frac{a_i}{a'}\right)}{\sqrt{\frac{8\pi G}{3c^2}e_i + \frac{\Lambda c^2}{3}\left(\frac{a_i}{a'}\right)^4}} = \int_0^t dt'. \quad (\text{A.4})$$

If $\Lambda > 0$, the solution for the scale factor is

$$a(t) = a_i \left(\frac{8\pi G e_i}{\Lambda c^4}\right)^{1/4} \left[\sinh\left(2\sqrt{\frac{\Lambda}{3}} ct\right) \right]^{1/2}, \quad (\text{A.5})$$

Using (A.5) in (A.1) we get the Hubble parameter

$$H(t) = \sqrt{\frac{\Lambda}{3}} c \coth\left(2\sqrt{\frac{\Lambda}{3}} ct\right), \quad (\text{A.6})$$

which, in the limit $\Lambda \rightarrow 0$, reduces to the standard expression $H(t) = 1/2t$. Inserting (A.6) into (A.1) we get the expression for $e(t)$

$$e(t) = \frac{\Lambda c^4}{8\pi G} \left[\sinh\left(2\sqrt{\frac{\Lambda}{3}} ct\right) \right]^{-2}. \quad (\text{A.7})$$

Another useful expression is the inverse of (A.6)

$$t = \left(4\sqrt{\frac{\Lambda}{3}}c\right)^{-1} \ln \left(\frac{H + \sqrt{\frac{\Lambda}{3}}c}{H - \sqrt{\frac{\Lambda}{3}}c}\right), \quad (\text{A.8})$$

which we have used in the cosmic time code to calculate the initial time for the calculation.

Finally, for completeness, we calculate the expression for the two cosmological horizons. From (A.6) we get a straightforward the expression for the Hubble horizon $R_H \equiv c/H$,

$$R_H(t) = \left(\frac{\Lambda}{3}\right)^{-\frac{1}{2}} \tanh \left(2\sqrt{\frac{\Lambda}{3}}ct\right). \quad (\text{A.9})$$

For the particle horizon, the calculation is more complicated. From the definition

$$R_h(t) \equiv a(t) \int_0^t \frac{cdt'}{a(t')}, \quad (\text{A.10})$$

we get

$$R_h(t) = \left[\sinh \left(2\sqrt{\frac{\Lambda}{3}}ct\right)\right]^{1/2} \int_0^t \frac{du}{\left[\sinh \left(2\sqrt{\frac{\Lambda}{3}}cu\right)\right]^{1/2}}, \quad (\text{A.11})$$

and, with the aid of integral tables, we get the final form of the solution

$$R_h(t) = \left(2\sqrt{\frac{\Lambda}{3}}\right)^{-1} \left[\sinh \left(2\sqrt{\frac{\Lambda}{3}}ct\right)\right]^{1/2} F(\phi, k) \quad (\text{A.12})$$

where $F(\phi, k)$ is an incomplete elliptic integral of the first type:

$$F(\phi, k) \equiv \int_0^\phi \frac{d\theta}{(1 - k^2 \sin^2 \theta)^{1/2}}, \quad (\text{A.13})$$

with

$$\phi = \arccos \left[\frac{1 - \sinh \left(2\sqrt{\frac{\Lambda}{3}}ct\right)}{1 + \sinh \left(2\sqrt{\frac{\Lambda}{3}}ct\right)} \right], \quad (\text{A.14})$$

and

$$k = \frac{1}{\sqrt{2}}. \quad (\text{A.15})$$

When $\Lambda < 0$, relations (A.5), (A.6) and (A.7) are unchanged apart from replacing the hyperbolic functions by the corresponding trigonometric ones. This is consistent with the oscillating behaviour of a universe with $\Lambda < 0$, characterized by a sequence of expanding and contracting phases.

References

- [1] Liddle A.R. & Lyth D.H. 2000 *Cosmological Inflation and Large-Scale Structure* Cambridge University Press
- [2] Zel'dovich Ya.B. & Novikov I.D. 1966 *Astron.Zh.* **43** 758 [*Sov.Astron.* **10** 602 (1967)]
- [3] Hawking S.W. 1971 *MNRAS* **152** 75
- [4] Carr B.J. & Hawking S.W. 1974 *MNRAS* **168**, 399
- [5] Nagatani Y. 1999 *Phys.Rev.D* **59** 041301
- [6] Cline D.B., Sanders D.A. & Hong W.P. 1997 *Astrophys. J.* **486** 169
- [7] Cline D.B., Matthey C. & Otwinowsky S. 1999 *Astrophys.J.* **527** 827
- [8] Green A.M. 2002 *Phys.Rev.D* **65** 027301
- [9] Carr B.J. 2003 *Lect. Notes Phys.* **631** 301
- [10] Barrau A., Blais D., Boudoul G. & Polarski D. 2003 *Phys. Lett. B* **551** 218
- [11] MacGibbon J.H. 1987 *Nature* **329** 308
- [12] Blais D., Kiefer C. & Polarski D. 2002 *Phys. Lett. B* **535** 11
- [13] Anshordi N., McDonald P., Spergel D.N. 2003 *Astrophys. J.* **594** L71
- [14] Carr B.J. 1975 *Astrophys.J.* **201** 1
- [15] Kim H.I. & Lee C.H. 1996 *Phys.Rev.D* **54** 6001
- [16] Nakamura T., Sasaki M., Tanaka T. & Thorne K.S. 1997 *Astrophys.J.Lett.* **487** L139
- [17] MACHO Collaboration, Alcock C. et al. 1996 *Astrophys.J.* **471** 774
- [18] Green A.M. & Jedamzik K. 2002 *Astron.Astrophys.* **395** 31
- [19] Rahvar S. 2003 *Int.J.Mod.Phys.D* **12** 45
- [20] Carr B.J., Gilbert J.H. & Lidsey J.E. 1994 *Phys.Rev.D* **50** 4853
- [21] Green A.M. & Liddle A.R. 1997 *Phys.Rev.D* **56** 6166
- [22] Liddle A.R. & Green A.M. 1998 *Phys.Rep.* **307** 125
- [23] Kribs G.D., Leibovitch A.K. & Rothstein I.Z. 1999 *Phys.Rev.D* **60** 103510
- [24] Bringmann T., Kiefer C. & Polarski D. 2002 *Phys.Rev.D* **65** 024008
- [25] Nadezhin D.K., Novikov I.D. & Polnarev A. G. 1978 *Astron.Zh.* **55** 216 [*Sov.Astron.* **22(2)** 129 (1978)]
- [26] May M.M. & White R.H. 1966 *Phys.Rev.* **141** 1232
- [27] Pondurets M.A. 1964 *Astron.Zh.* **41** 1090 [*Sov.Astron.* **8** 868 (1965)]
- [28] Bicknell G.V. & Henriksen R. N. 1979 *Astrophys.J.* **232** 670
- [29] Niemeyer J.C. & Jedamzik K. 1998 *Phys.Rev.Lett.* **80** 5481
- [30] Niemeyer J.C. & Jedamzik K. 1999 *Phys.Rev.D* **59** 124013
- [31] Choptuik M.W. 1993 *Phys.Rev.Lett.* **70** 9
- [32] Evans C.R. & Coleman J.S. 1994 *Phys.Rev.Lett.* **72** 1782
- [33] Gundlach C. 1999 *Living Rev.Rel.* [<http://www.livingreviews.org/lrr-1999-4>]
- [34] Hernandez W.C. & Misner C.W. 1966 *Astrophys.J.* **143** 452
- [35] Harada T., Goymer C. & Carr B.J. 2002 *Phys. Rev. D* **66** 104023

- Harada T. & Carr B.J. 2004 astro-ph/0412134
- Harada T. & Carr B.J. 2004 astro-ph/0412135
- [36] Hawke I. & Stewart J. M. 2002 *Class. Quantum Grav.* **19** 3687
- [37] Shibata M. & Sasaki M. 1999 *Phys.Rev.D* **60** 084002
- [38] Green A.M., Liddle A.R., Malik K.A., Sasaki M. 2004 *Phys.Rev.D*, **70**, 041502
- [39] Miller J.C. & Motta S. 1989 *Class. Quantum Grav.* **6** 185
- [40] Misner C.W. & Sharp D.H. 1964 *Phys.Rev* **136** B571
- [41] Miller J.C. & Sciama D.W. 1980 in *General Relativity and Gravitation: one hundred years after the birth of Albert Einstein - Vol.2* ed. Held A. (Plenum Press: New York), p. 359
- [42] Baumgarte T.W., Shapiro S.L. & Teukolsky S.A. 1995 *Astrophys.J.* **443** 717
- [43] Miller J.C. & Pantano O. 1990 *Phys.Rev.D* **42** 3334
- [44] Miller J.C. & Rezzolla L. 1995 *Phys.Rev.D* **51** 4017
- [45] Padmanabhan T. 1993 *Structure Formation in the Universe* Cambridge University Press
- [46] Koike T, Hara T. & Adachi S. 1995 *Phys.Rev.Lett.* **74** 5170
- [47] Jedamzik K. & Niemeyer J.C. 1999 *Phys.Rev.D* **59** 124014